Optimal Service Restoration in Active Distribution Networks Considering Microgrid Formation and Voltage Control Devices

Leonardo H. Macedo, *Member, IEEE*, Gregorio Muñoz-Delgado, *Member, IEEE*, Javier Contreras, *Fellow, IEEE*, and Rubén Romero, *Senior Member, IEEE*

***Abstract*—This paper presents a new mixed-integer linear programming model for the optimal restoration of active distribution networks during permanent fault events considering not only network reconfiguration but also the islanded operation of distributed generation, thereby giving rise to the formation of microgrids. To that end, the proposed approach accounts for both the black-start capacity of generators and the connection of multiple generators to the same microgrid. Moreover, voltage control devices such as substations' on-load tap changers, voltage regulators, and capacitor banks are also considered in the formulation. The model is driven by the minimization of the out-of-service load after single or multiple faults in the network using the minimum number of switching operations and modifications in the statuses of the voltage control devices. The proposed model is implemented in the mathematical modeling language AMPL and solved with the CPLEX solver. Tests are conducted using a 53-node distribution system considering different fault locations. Numerical results show the relevant effect of microgrid formation and voltage control in the restoration process. Simulations also prove the effective performance of the proposed approach in terms of computation time.**

***Keywords*—Active distribution systems, distributed generation, mixed-integer linear programming, service restoration, voltage control.**

NOMENCLATURE

Indices:

i, j, n	Indices for nodes
ij, ji	Indices for branches
k	Index for capacitor bank (CB) modules
l	Index for linearization blocks

Sets:

Ω_B	Set of all branches in the system, including the artificial ones, $\Omega_B = \Omega_B^R \cup \Omega_{SW}^F$
Ω_B^R	Set of real branches
Ω_B^{VR}	Set of branches with a voltage regulator (VR)
Ω_N	Set of all nodes of the system, including the artificial substation node, $\Omega_N = \Omega_N^R \cup \Omega_N^F$
Ω_N^{CB}	Set of nodes with CBs
Ω_N^D	Set of demand nodes, $\Omega_N^D = \Omega_N^R \backslash \Omega_N^{SS}$
Ω_N^{DG}	Set of nodes with distributed generators (DGs)
Ω_N^{DG+}	Set of nodes with DGs with black-start capacity
Ω_N^F	Set containing only the artificial substation node
Ω_N^{OLTC}	Set of substations' on-load tap changer (OLTC) nodes
Ω_N^R	Set of real nodes
Ω_N^{SS}	Set of real substation nodes
Ω_{SW}	Set of all branches with a switch in the system, $\Omega_{SW} = \Omega_{SW}^R \cup \Omega_{SW}^F$
Ω_{SW}^C	Set of real branches with a closed switch in the pre-fault state
Ω_{SW}^F	Set of artificial branches, all with switches
Ω_{SW}^O	Set of real branches with an open switch in the pre-fault state
Ω_{SW}^R	Set of all real branches of the system with a switch, $\Omega_{SW}^R = \Omega_{SW}^O \cup \Omega_{SW}^C$
$\Omega_{\mathbb{S}}^F$	Set of sections under fault
$\Omega_{\mathbb{S}}^R$	Set of all sections in the system

Parameters:

$\overline{\Delta}_i^{OLTC}$	Maximum regulation for the OLTC at substation node i
$\overline{\Delta}_{ij}^{S}$	Length of each block of the linearization of the squares of the power flows on branch ij
$\overline{\Delta}_{ij}^{VR}$	Maximum regulation for the VR at branch ij
Φ_i	Indicates whether node i has a DG, $\Phi_i = 1$, or not, $\Phi_i = 0$
Λ	Number of blocks of the piecewise linearization
Ψ_i^{CB}	Number of modules of the CB at node i operating in the pre-fault condition
Ψ_i^{DGp}, Ψ_i^{DGq}	Pre-fault active/reactive generations of the DG at node i
Ψ_i^{OLTC}	Pre-fault value of V_i^{SQ} for the substation at node i
Ψ_{ij}^{VR}	Pre-fault value of δ_{ij}^{VR} for branch ij with a VR
α_i^Z, α_i^I, α_i^P	Participation factors of constant impedance/current/power loads in the active power demand at node i
β_i^Z, β_i^I, β_i^P	Participation factors of constant impedance/current/power loads in the reactive power demand at node i
ϑ_i	Estimate of the voltage magnitude at node i, obtained from the pre-fault operation
κ_i^{CB}	Cost of changing the operational status of a CB module at node i
κ_i^{DGp}, κ_i^{DGq}	Cost of modifying the active/reactive output of the DG at node i
κ_i^{LS}	Cost of not supplying the demand (load shedding) at node i
κ^{MG}	Cost of forming a microgrid
κ_i^{OLTC}	Cost of modifying the operation of the OLTC at node i
κ_{ij}^{SW}	Switching operation cost of branch ij
κ_{ij}^{VR}	Cost of modifying the operation of the VR at branch ij
μ_i^{DG}	Reduction factor for the generation capacity of the main DG of a microgrid with black-start capacity located at node i
ρ_i^{DG}	Ramp-up rate limit of the DG at node i
$\bar{\tau}_i^{cap}$, $\bar{\tau}_i^{ind}$	Limits for the capacitive/inductive power factors of the DG at node i
B_i^{CB}	Susceptance of a module of the CB at node i
$\overline{I}_{ij}$	Current capacity of branch ij
M_{ij}	Big-M parameter for the voltage drop calculation on branch ij
M_i^P, M_i^Q	Big-M parameters used in the calculation of the active/reactive load at node i
N_i^{CB}	Number of modules of the CB at node i
P_i^D, Q_i^D	Active/reactive demands in node i at nominal voltage
R_{ij}, X_{ij}, Z_{ij}	Resistance/reactance/magnitude of the impedance of branch ij
$\overline{S}_i^{DG}$	Apparent power capacity of the DG at node i
$\overline{S}_i^{SS}$	Apparent power capacity of the substation at node i
V^N, $\underline{V}$, $\overline{V}$	Nominal/minimum/maximum voltage magnitudes at node i
$m_{ij,l}$	Slope of block l of the piecewise linearization for branch ij
$\mathbb{S}_i$	Section which contains node i

Continuous variables:

$\Delta_{ij,l}^P$, $\Delta_{ij,l}^Q$	Discretization variables related to block l of the active/reactive power flows on branch ij
Δ_{ij}^{VR}	Regulation of the VR at branch ij
$\hat{\delta}_i^{DGp}$, $\hat{\delta}_i^{DGq}$	Modification of the active/reactive power dispatch of the DG at node i
$\hat{\delta}_i^{OLTC}$	Modification of the operation of the OLTC at node i
$\hat{\delta}_{ij}^{VR}$	Modification of the operation of the VR at branch ij

This work was supported in part by the Coordination for the Improvement of Higher Education Personnel (CAPES)—Finance Code 001, the Brazilian National Council for Scientific and Technological Development (CNPq), grant 305852/2017-5, and the São Paulo Research Foundation (FAPESP), under grants 2015/21972-6, 2018/20355-1, and 2019/19632-3, and in part by the Ministry of Science, Innovation and Universities of Spain, under Projects RTI2018-096108-A-I00 and RTI2018-098703-B-I00 (MCIU/AEI/FEDER, UE), and by the Universidad de Castilla-La Mancha, under grant 2021-GRIN-30952.

L. H. Macedo and R. Romero are with the Department of Electrical Engineering, São Paulo State University, Ilha Solteira, SP 15385-000 Brazil (e-mails: leohfmp@ieee.org; ruben.romero@unesp.br).

G. Muñoz-Delgado and J. Contreras are with the Escuela Técnica Superior de Ingeniería Industrial, Universidad de Castilla-La Mancha, 13071 Ciudad Real, Spain (e-mails: Gregorio.Munoz@uclm.es; Javier.Contreras@uclm.es).

δ_{ij}^{VR} Auxiliary variable used in the model of the VRs (for a branch without a VR, $\delta_{ij}^{VR}=0$)

ξ_{ij} Slack variable used in the calculation of the voltage drop of a branch with a switch according to its operation (for a branch without a switch, $\xi_{ij}=0$)

I_{ij}^{SQ} Square of the current magnitude on branch ij

P_{ij}, Q_{ij} Active/reactive power flows on branch ij

P_{ij}^{+}, P_{ij}^{-} Nonnegative variables used to represent the active power flows on branch ij

$\hat{P}_i^D$, $\hat{Q}_i^D$ Voltage-dependent active/reactive power demands at node i

P_i^{DG}, Q_i^{DG} Active/reactive power generations of the DG at node i

P_i^{SS}, Q_i^{SS} Active/reactive power injections of the substation at node i

Q_{ij}^{+}, Q_{ij}^{-} Nonnegative variables used to represent the reactive power flows on branch ij

Q_i^{CB} Total reactive power injection of the CB installed at node i

V_i, V_i^{SQ} Voltage magnitude and its square value at node i

a_{ij} Tap of the VR on branch ij

$q_{i,k}^{CB}$ Reactive power injected by module k of the CB at node i

Integer-valued continuous variables:

$\hat{\delta}_i^{CB}$ Modification in the number of CB modules connected at node i

$\hat{\delta}_{ij}^{SW}$ Indicates a switching operation at branch ij

f_{ij}^{e} Artificial flow on branch ij used to guarantee the radiality of the main grid and each microgrid

f_{ij}^{f} Artificial flow on branch ij used to guarantee that the de-energized nodes are disconnected from the main grid

f_{ij}^{r} Artificial flow on branch ij used in the constraints related to the formation of microgrids

g_i^e Artificial generation of the substation at node i used to guarantee the radiality of the main grid and each microgrid

g_i^f Generation at the artificial substation at node i used to guarantee that the de-energized nodes are disconnected from the main grid

g_i^r Artificial generation at node i used in the constraints related to the formation of microgrids

z_{ij} Auxiliary variable used in the linearization of the product $\left(1-y_{\mathbb{S}_i}^{LS}\right)\left(1-y_{\mathbb{S}_j}^{LS}\right)$

Binary variables:

λ_i^{DG} Indicates that at least one DG with black-start capacity is operating in a microgrid that contains node i when $\lambda_i^{DG}=1$

w_{ij}^{SW} Indicates whether the switch of branch ij is open, $w_{ij}^{SW}=0$, or closed, $w_{ij}^{SW}=1$. For the branches without a switch, $w_{ij}^{SW}=1$

$x_{i,k}^{CB}$ Operational state of module k of the CB at node i: $x_{i,k}^{CB}=1$ if the module is connected and $x_{i,k}^{CB}=0$, otherwise

$y_{\mathbb{S}_i}^{LS}$ Indicates whether section $\mathbb{S}_i$, that contains node i, is energized, $y_{\mathbb{S}_i}^{LS}=1$, or not, $y_{\mathbb{S}_i}^{LS}=0$

I. Introduction

This section is divided into four subsections, namely motivation, literature survey, contributions, and paper organization.

A. Motivation

After the occurrence of a permanent fault in a radial distribution system, all sections downstream of the fault are de-energized. A section of a distribution system is formed by the nodes and branches that cannot be disconnected from each other through switching operations. Subsequently, the faulted sections of the network must be isolated for repair whereas the rest of the de-energized sections are candidates to be restored [1]. The objective of service restoration is to reduce the negative impact of permanent faults. It must be executed without violating the physical and operational limits of the equipment available in the network so that quality and safety aspects are not compromised [2]. These requirements, together with the network operation model, lead to a complex mixed-integer nonlinear programming problem, which is difficult to solve even for small instances.

B. Literature Survey

Different approaches are available in the literature to solve this problem, usually considering that the network topology after reconfiguration must be radial and connected [3], [4]. Nevertheless, in addition to network reconfiguration, new restoration strategies are emerging for active distribution networks with DGs such as microgrid formation, in which the network is divided into microgrids after the occurrence of single or multiple faults [5].

References [6]–[13] solve the service restoration problem considering the possibility of forming microgrids. However, these works disregard the possibility of network reconfiguration. In [6], a heuristic approach for island partition in radial distribution systems based on the solution of tree knapsack problems is presented. In [7], a mixed-integer linear programming (MILP) formulation is proposed for microgrids formation in radial systems after natural disasters considering that each microgrid is supplied by only one DG and that the load at the nodes can be disconnected. Reference [8] proposes a heuristic method for the island partition of distribution networks for service restoration that uses graph-theory-based algorithms for the islands formation and an optimal power flow algorithm together with load management strategies to ensure the adequate operation of the system. This approach considers load shedding at the nodes with uncontrollable loads as a strategy to satisfy the operational constraints of the system. Reference [9] proposes an evolutionary metaheuristic algorithm for the partition of distribution networks after large-scale events. It divides the distribution system into microgrids with the objective of minimizing the demand not supplied. The approach also performs the allocation of DGs in the network. Reference [10] proposes a heuristic method based on Dijkstra's algorithm and fuzzy logic to re-energize the maximum number of critical loads with microgrids after the occurrence of severe faults that disconnect the distribution network from the transmission system. Reference [11] analyses the impact of a demand response program on the resilience of distribution systems allowing the dynamic formation of microgrids during the day, i.e., for each period of time of a day, a different group of microgrids is formed in the network. The approach uses an evolutionary metaheuristic to solve the problem considering two objective functions: improve the resilience of the system and its voltage profile. Reference [12] presents a mixed-integer second-order cone programming model for the restoration of distribution systems considering microgrid formation and demand-side management. Finally, reference [13] proposes a two-stage mathematical programming-based method for service restoration in distribution systems considering microgrid formation.

Several heuristics, metaheuristics, and mathematical programming models have been presented in the literature to solve the service restoration problem considering both network reconfiguration and microgrid formation [14]–[20]. Note that, in contrast to mathematical programming models, the radiality and connectivity constraints can be easily included within the solution process of heuristic and metaheuristic models. However, such heuristic and metaheuristic optimization methods are unable to acknowledge the attainment of global optimality [21]. A heuristic approach based on spanning tree search is presented in [14] for the restoration of distribution systems considering distributed energy resources for maximizing the restored load and minimizing the number of switching operations after a fault. Reference [15] proposes a heuristic method for the restoration of critical loads through microgrid formation considering network reconfiguration in

TABLE I
PROPOSED APPROACH VERSUS THE RELATED LITERATURE

Reference	Reconfiguration	Microgrid formation	Voltage control	Mathematical programming-based
[3], [4]	✓	✗	✗	✓
[6], [8], [9], [10], [11]	✗	✓	✗	✗
[7], [12], [13]	✗	✓	✗	✓
[14], [15], [17], [18], [19]	✓	✓	✗	✗
[16], [20]	✓	✓	✗	✓
[25]	✓	✗	✓	✗
[26]	✓	✗	✓	✓
This paper	✓	✓	✓	✓

distribution systems. Reference [16] presents an MILP model for service restoration considering microgrid formation, network topology changes, including both radial and meshed configurations, and mobile DGs. Reference [17] presents a heuristic approach for service restoration considering reconfiguration and renewable DG islanding. To deal with the uncertainties of the renewable generation, the authors used a method called *stochastic response surface method*. Reference [18] presents a framework for service restoration considering the market aspects of the problem. Reference [19] proposes a method to solve the service restoration problem that uses a mixed-integer semidefinite programming model for the coordination of DGs and energy storage systems in microgrids. Reference [20] is one of the few works that have simultaneously considered both network reconfiguration and microgrid formation within a mathematical programming-based approach to solve the restoration problem. The presented model is based on a directed multicommodity flow formulation to ensure the radiality of the network.

Modern distribution systems also include remotely operated voltage control devices, such as VRs, substations' OLTCs, and CBs, that add flexibility to the operation of the system, improving the voltage profile and minimizing losses [22]–[24]. The control of such devices can be considered in the service restoration problem to increase the amount of load restored. Regarding the voltage control in the service restoration problem, reference [25] presents a tabu-search algorithm that optimizes the network topology and the operation of DGs, VRs, and CBs for obtaining optimized solutions for this problem. Reference [26] proposes a mixed-integer second-order cone programming model for the problem of service restoration with voltage control, also considering that the resulting network topology should be radial and connected. It is worth mentioning that both references [25] and [26] do not consider microgrid formation. Moreover, as can be verified in [27], [28], voltage control is usually disregarded in the service restoration problem, especially when microgrid formation is considered.

Table I summarizes the main features of this work and the state of the art [3], [4], [6]–[20], [25], and [26]. In this table, symbols "✓" and "✗" respectively indicate whether a particular aspect is considered or not. As can be observed in this table (i) the possibility of changing the topology of the network is disregarded in [6]–[13], (ii) microgrid formation is not allowed in [3], [4], [25] and [26], (iii) voltage control is only considered in [25] and [26], and (iv) heuristics and metaheuristics are extensively used in the related literature. In addition, it can be verified that in [16] and [20], where mathematical-programming-based models are used, a simplifying assumption is made by considering the possibility of disconnecting the loads from the nodes to ensure the radiality of the system, i.e., there is not the possibility of electrically isolating sections of the system from the main grid (see Fig. 2(d) and the related text for discussion about this subject). Finally, it can be observed that the works in [4], [6]–[8], [10], [13], [14], [16], [17], [19], and [20] assume that each line of the distribution system is equipped with two switches that can be used to completely isolate the fault, which may not be practical in many real systems.

This work is an extension of [1] with the following improvements: (i) the incorporation of a nomenclature section, (ii) a deeper bibliographical review of the problem, (iii) a detailed description of the service restoration process in a newly added section, (iv) an extended formulation that considers the minimization of the number of microgrids formed maintaining a reserve of capacity for the DGs operating in microgrids, (v) further and improved discussion and explanation about the formulation, and (vi) extended and improved presentation of the results.

It should be mentioned that, as done in all papers shown in Table I, frequency control of the microgrids is not considered in this work. The dynamics of the system [29] should be considered in another stage of the restoration procedure. Besides that, the synchronization of the microgrids with the main grid after the faults are cleared is also outside the scope of this paper.

C. Contributions

The main contribution of this paper is the formulation of a new MILP model to solve the problem of the optimal restoration of active distribution systems considering network reconfiguration, microgrid formation, and voltage control simultaneously, with the following benefits: (i) realistic considerations of the structure of distribution systems, flexible application, and precise results, (ii) efficient computational behavior with conventional MILP solvers, and (iii) convergence to optimality ensured by classical optimization techniques. In addition, from the analysis of the results, service restoration strategies for active distribution networks can be defined. The formulation also ensures that each portion of the system will present radial topology and allows sections to remain de-energized so that others can be restored. Also, the number of DGs in each microgrid is defined by the model, which also accounts for the black-start capacity of different DGs and a security reserve for the capacity of the DGs operating in a microgrid, differently from [7], for example, which considers only one DG operating in each microgrid.

D. Organization of the Manuscript

The rest of this work is structured as follows. The modeling framework for the service restoration process is described in Section II. Section III presents the problem formulation. In Section IV, the results obtained for a 53-node test system are reported and analyzed. Finally, relevant conclusions are drawn in Section V.

II. MODELING FRAMEWORK FOR SERVICE RESTORATION

The steps for service restoration in active distribution networks considering microgrid formation and voltage control are described below:

1) The first protective device upstream of the fault actuates to isolate the fault from the substation as soon as it occurs in a section of a distribution system. Additionally, all distributed generators (DGs) in the isolated sections are disconnected from the grid. As a result, the power supply is interrupted to all sections downstream of the protective device that actuated. The faulted section is isolated so that it may be repaired. Sections that were not affected by a fault must remain energized during the service restoration procedure;

2) The de-energized sections for which the service can be restored, as well as the available lines and switches, DGs, and voltage control devices, such as, capacitor banks (CBs), substations' on-load tap changers (OLTCs), and voltage regulators (VRs), are identified. The section directly affected by the fault and the protective and switching devices used to isolate it cannot be employed in the restoration process;
3) A service restoration strategy identifies the de-energized sections of the system that may be reconnected to the main grid or be operated in microgrid mode without violating operational limits. The restoration strategy should also determine the procedures that must be performed to restore service to these sections;
4) The restoration plan is then carried out by modifying the switches' operational statuses, redispatching the DGs, and adjusting the voltage control devices;
5) Finally, after the isolated fault has been cleared, the system's regular pre-fault operational condition is restored.

The distribution system operator may consider a variety of actions in Step 3) to restore the supply to the greatest possible number of customers or, as considered in this article, to minimize the out-of-service load. Moreover, several service restoration strategies may be used, as discussed in Subsection I-B.

Finally, it is worth mentioning that remotely operated voltage control devices and switches allow the effective application of the proposed approach in distribution systems. As discussed in [22]–[24], this type of equipment should be commonly present in modern smart grids. Moreover, remote monitoring and control of DGs also facilitate the implementation of the restoration procedure [15]. Finally, it should be mentioned that the computational times to obtain solutions for the restoration problem in Step 3) must be adequate for the time frame of the restoration procedure, which depends on the time required to clear the faults. In the literature, ten minutes has been considered a reasonable time to obtain a solution for the problem [30].

III. MILP Problem Formulation

The proposed MILP formulation is presented below.

A. Objective Function

The formulation optimizes the service restoration problem by minimizing the total restoration cost, which is obtained by converting the power of the de-energized loads and the performed actions into costs. Equation (1) presents the objective function of the problem.

$$\begin{aligned}\text{minimize}\,\psi = &\sum_{i\in\Omega_N^D|\mathbb{S}_i\notin\Omega_{\mathbb{S}}^F}\kappa_i^{LS}P_i^D\big(1-y_{\mathbb{S}_i}^{LS}\big)+\sum_{ij\in\Omega_{SW}^R}\kappa_{ij}^{SW}\hat{\delta}_{ij}^{SW}+\\ &\sum_{i\in\Omega_N^{DG}}\Big(\kappa_i^{DGp}\hat{\delta}_i^{DGp}+\kappa_i^{DGq}\hat{\delta}_i^{DGq}\Big)+\sum_{i\in\Omega_N^{CB}}\kappa_i^{CB}\hat{\delta}_i^{CB}+\\ &\sum_{i\in\Omega_N^{OLTC}}\kappa_i^{OLTC}\hat{\delta}_i^{OLTC}+\sum_{ij\in\Omega_B^{VR}}\kappa_{ij}^{VR}\hat{\delta}_{ij}^{VR}+\kappa^{MG}\sum_{i\in\Omega_N^{DG+}}\lambda_i^{DG}\end{aligned}\quad(1)$$

The first term of the objective function ψ, shown in (1), is the cost of the total active load not supplied. Additional constraints ensure that, if the load of a section is not supplied, then this section must be completely disconnected from the system. The second term is the cost of the switching operations. The third term is the cost of modifications on the active and reactive power dispatch values of the DGs. The fourth term is the cost of modifying the number of CBs in operation. The fifth and sixth terms are the costs of modifying the operation of OLTCs and VRs, respectively. The last term is the cost of forming microgrids.

B. Linearized Power Flow Constraints

The ac operation of the system is represented by the power flow equations (2)–(12).

$$\sum_{ji\in\Omega_B^R}P_{ji}-\sum_{ij\in\Omega_B^R}\big(P_{ij}+R_{ij}I_{ij}^{SQ}\big)+P_i^{SS}+P_i^{DG}=\hat{P}_i^D \quad(2)$$

$$\sum_{ji\in\Omega_B^R}Q_{ji}-\sum_{ij\in\Omega_B^R}\big(Q_{ij}+X_{ij}I_{ij}^{SQ}\big)+Q_i^{SS}+Q_i^{DG}+Q_i^{CB}=\hat{Q}_i^D \quad(3)$$

$$\forall i\in\Omega_N^R$$

$$V_i^{SQ}-V_j^{SQ}+\delta_{ij}^{VR}+\xi_{ij}=2(R_{ij}P_{ij}+X_{ij}Q_{ij})+Z_{ij}^2I_{ij}^{SQ} \quad(4)$$

$$\forall ij\in\Omega_B^R$$

$$|\xi_{ij}|\le M_{ij}(1-w_{ij}^{SW}) \qquad \forall ij\in\Omega_B^R \quad(5)$$

$$\vartheta_j^2I_{ij}^{SQ}=\sum_{l=1}^{\Lambda}m_{ij,l}(\Delta_{ij,l}^P+\Delta_{ij,l}^Q) \qquad \forall ij\in\Omega_B^R \quad(6)$$

$$P_{ij}=P_{ij}^+-P_{ij}^- \qquad \forall ij\in\Omega_B^R \quad(7)$$

$$Q_{ij}=Q_{ij}^+-Q_{ij}^- \qquad \forall ij\in\Omega_B^R \quad(8)$$

$$P_{ij}^++P_{ij}^-=\sum_{l=1}^{\Lambda}\Delta_{ij,l}^P \qquad \forall ij\in\Omega_B^R \quad(9)$$

$$Q_{ij}^++Q_{ij}^-=\sum_{l=1}^{\Lambda}\Delta_{ij,l}^Q \qquad \forall ij\in\Omega_B^R \quad(10)$$

$$0\le\Delta_{ij,l}^P\le\overline{\Delta}_{ij}^S \qquad \forall ij\in\Omega_B^R, l\in\{1,\cdots,\Lambda\} \quad(11)$$

$$0\le\Delta_{ij,l}^Q\le\overline{\Delta}_{ij}^S \qquad \forall ij\in\Omega_B^R, l\in\{1,\cdots,\Lambda\} \quad(12)$$

Constraints (2) and (3) represent the application of Kirchhoff's current law to the system. Note that these equations include the active and reactive power injections of the DGs and the reactive power injections of the CBs. Besides that, as can be seen in Subsection III-C, the values of the loads depend on the voltage magnitudes at the nodes and the operating statuses of the sections of the system to which they belong. Constraint (4) represents the application of Kirchhoff's voltage law to the system. The slack variable ξ_{ij} in (4) is calculated in (5) according to the value of w_{ij}^{SW}, with $M_{ij}=\big(\overline{V}^2-\underline{V}^2\big)$ for a branch without a VR, and $M_{ij}=\big(\overline{V}^2-\underline{V}^2\big)+\overline{\Delta}_{ij}^{VR}\left(2+\overline{\Delta}_{ij}^{VR}\right)\overline{V}^2$ for a branch with a VR (see Subsection III-F for more information related to the formulation of VRs). Note that if $w_{ij}^{SW}=1$, then $\xi_{ij}=0$ and (4) is applied to the system. Otherwise, if $w_{ij}^{SW}=0$, the values of the square of the voltage magnitudes in (4) are independent. Finally, the piecewise linearization (6)–(12) provides the values of I_{ij}^{SQ} for the branches, in which the length of each block of the linearization of the squares of the power flows is $\overline{\Delta}_{ij}^S=\overline{V}\overline{I}_{ij}/\Lambda$ and the slope of each block is $m_{ij,1}=(5/6)\overline{\Delta}_{ij}^S$ and $m_{ij,l}=(2l-1)\overline{\Delta}_{ij}^S$, for $l>1$ [31]. It should be noted that the greater the value of Λ, the more precise is the approximation, at the expense of increasing the size and computational burden of the model.

C. Load Model

The load is modeled using the voltage-dependent polynomial ZIP model [32]. Constraints (13)–(16) represent the values of the loads according to the voltage magnitude at node i, calculated in (17), and the state of the binary variable $y_{\mathbb{S}_i}^{LS}$, defined in (18).

$$\left|\hat{P}_i^D-P_i^D\left[\alpha_i^Z\frac{V_i^{SQ}}{(V^N)^2}+\alpha_i^I\frac{V_i}{V^N}+\alpha_i^P\right]\right|\le M_i^P(1-y_{\mathbb{S}_i}^{LS})\ \forall i\in\Omega_N^D \quad(13)$$

$$|\hat{P}_i^D|\le M_i^Py_{\mathbb{S}_i}^{LS} \qquad \forall i\in\Omega_N^D \quad(14)$$

$$\left|\hat{Q}_i^D-Q_i^D\left[\beta_i^Z\frac{V_i^{SQ}}{(V^N)^2}+\beta_i^I\frac{V_i}{V^N}+\beta_i^P\right]\right|\le M_i^Q(1-y_{\mathbb{S}_i}^{LS})\ \forall i\in\Omega_N^D \quad(15)$$

$$\left|\hat{Q}_i^D\right|\le M_i^Qy_{\mathbb{S}_i}^{LS} \qquad \forall i\in\Omega_N^D \quad(16)$$

$$V_i = \sqrt{\frac{\overline{V}+\underline{V}}{2}} + \frac{1}{2\sqrt{\frac{\overline{V}+\underline{V}}{2}}}\left(V_i^{SQ} - \frac{\overline{V}+\underline{V}}{2}\right) \qquad \forall i \in \Omega_N^D \quad (17)$$

$$y_{\mathbb{S}_i}^{LS} \in \{0,1\} \qquad \forall i \in \Omega_N^D \quad (18)$$

The big-M formulation (13)–(16) provides the values of the active and reactive power demands, respectively, according to the value of $y_{\mathbb{S}_i}^{LS}$. The value of V_i^{SQ} is available directly from the formulation, however, V_i needs to be calculated. Constraint (17) calculates $V_i = \sqrt{V_i^{SQ}}$ using a Taylor's series approximation at $V_i^{SQ} = (\overline{V} + \underline{V})/2$, ignoring the higher order terms. In this approximation, for $\underline{V} = 0.95$ p.u. and $\overline{V} = 1.05$ p.u., the maximum error is 0.13% for $V_i^{SQ} = \underline{V}^2$. For each $i \in \Omega_N^D$, the values of M_i^P and M_i^Q are calculated as $P_i^D\left[\alpha_i^Z \frac{\overline{V}^2}{(V^N)^2} + \alpha_i^I \frac{\overline{V}}{V^N} + \alpha_i^P\right]$ and $Q_i^D\left[\beta_i^Z \frac{\overline{V}^2}{(V^N)^2} + \beta_i^I \frac{\overline{V}}{V^N} + \beta_i^P\right]$, respectively. These values are defined so that V_i^{SQ} and V_i are not constrained by (13) and (15) when $y_{\mathbb{S}_i}^{LS} = 0$.

D. Distributed Generators Model

The operation of the DGs is modeled in (19)–(38).

$$0 \le P_i^{DG} \le \overline{S}_i^{DG} y_{\mathbb{S}_i}^{LS} \quad (19)$$

$$|Q_i^{DG}| \le \overline{S}_i^{DG} y_{\mathbb{S}_i}^{LS} \quad (20)$$

$$|Q_i^{DG}| \le \sqrt{2}\,\overline{S}_i^{DG} y_{\mathbb{S}_i}^{LS} - P_i^{DG} \quad (21)$$

$$|Q_i^{DG}| \le \frac{1}{\sin\left(\frac{\pi}{8}\right)} \overline{S}_i^{DG} y_{\mathbb{S}_i}^{LS} - \tan\left(\frac{3\pi}{8}\right) P_i^{DG} \quad (22)$$

$$|Q_i^{DG}| \le \frac{1}{\sin\left(\frac{3\pi}{8}\right)} \overline{S}_i^{DG} y_{\mathbb{S}_i}^{LS} - \tan\left(\frac{\pi}{8}\right) P_i^{DG} \quad (23)$$

$$-P_i^{DG}\tan(\cos^{-1}(\bar{\tau}_i^{cap})) \le Q_i^{DG} \le P_i^{DG}\tan(\cos^{-1}(\bar{\tau}_i^{ind})) \quad (24)$$

$$\left|\Psi_i^{DGp} - P_i^{DG}\right| \le \hat{\delta}_i^{DGp} \quad (25)$$

$$\left|\Psi_i^{DGq} - Q_i^{DG}\right| \le \hat{\delta}_i^{DGq} \quad (26)$$

$$-\Psi_i^{DGp} \le P_i^{DG} - \Psi_i^{DGp} \le \rho_i^{DG} \quad \forall i \in \Omega_N^{DG} \quad (27)$$

$$\sum_{ji \in \Omega_B^R} f_{ji}^r - \sum_{ij \in \Omega_B^R} f_{ij}^r + g_i^r = \Phi_i y_{\mathbb{S}_i}^{LS} \qquad \forall i \in \Omega_N^R \quad (28)$$

$$\left|f_{ij}^r\right| \le |\Omega_N^{DG}| w_{ij}^{SW} \qquad \forall ij \in \Omega_B^R \quad (29)$$

$$g_i^r = 0 \qquad \forall i \in [\Omega_N - (\Omega_N^{SS} \cup \Omega_N^{DG+})] \quad (30)$$

$$0 \le g_i^r \le |\Omega_N^{DG}| \qquad \forall i \in \Omega_N^{SS} \quad (31)$$

$$0 \le g_i^r \le \lambda_i^{DG} |\Omega_N^{DG}| \qquad \forall i \in \Omega_N^{DG+} \quad (32)$$

$$0 \le P_i^{DG} \le \overline{S}_i^{DG}(1 - \mu_i^{DG}\lambda_i^{DG}) \quad (33)$$

$$|Q_i^{DG}| \le \overline{S}_i^{DG}(1 - \mu_i^{DG}\lambda_i^{DG}) \quad (34)$$

$$|Q_i^{DG}| \le \sqrt{2}\,\overline{S}_i^{DG}(1 - \mu_i^{DG}\lambda_i^{DG}) - P_i^{DG} \quad (35)$$

$$|Q_i^{DG}| \le \frac{1}{\sin\left(\frac{\pi}{8}\right)} \overline{S}_i^{DG}(1 - \mu_i^{DG}\lambda_i^{DG}) - \tan\left(\frac{3\pi}{8}\right) P_i^{DG} \quad (36)$$

$$|Q_i^{DG}| \le \frac{1}{\sin\left(\frac{3\pi}{8}\right)} \overline{S}_i^{DG}(1 - \mu_i^{DG}\lambda_i^{DG}) - \tan\left(\frac{\pi}{8}\right) P_i^{DG} \quad \forall i \in \Omega_N^{DG+} \quad (37)$$

$$\lambda_i^{DG} \in \{0,1\} \qquad \forall i \in \Omega_N^{DG+} \quad (38)$$

The set of constraints (19)–(23) is a linearization for the apparent power capacity of the DGs, according to the status of the respective section. Constraint (24) represents the capacitive and inductive power factor limits for the operation of the DGs. Fig. 1(a) illustrates the linearization of the capacity curve of the DGs. Constraints (25) and (26) are used to calculate the changes of the active and reactive power generations of the DGs between the pre-fault and the restored states. Constraint (27) is the ramp-up rate limit of the DGs, in which $0 \le \rho_i^{DG} \le \overline{S}_i^{DG} - \Psi_i^{DGp}$.

Constraints (28)–(32) require that there must exist a path between a substation or a DG with black-start capacity and a DG without black-start capacity so that the latter can operate. Constraint (28) creates artificial demands at the nodes with DGs, that can only be supplied by artificial generations generated at the real substations or nodes with DGs with black-start capacity, as defined in (30)–(32). Constraint (29) limits the artificial flows on the branches of the system according to the states of the switches. Note that in (32), a DG with black-start capacity can only have an artificial generation if $\lambda_i^{DG} = 1$. Since λ_i^{DG} is minimized in the objective function, one DG with black-start capacity will have $\lambda_i^{DG} = 1$ in each microgrid.

Constraints (33)–(37) require that in each microgrid, one DG with black-start capacity must maintain a reserve of capacity of μ_i^{DG}. Equation (38) defines the binary nature of the variable λ_i^{DG}.

E. Capacitor Banks Model

The operation of the CBs is formulated using a voltage-dependent model, as presented in (39)–(44). Fig. 1(b) illustrates the model of the CBs.

$$Q_i^{CB} = \sum_{k=1}^{N_i^{CB}} q_{i,k}^{CB} \qquad \forall i \in \Omega_N^{CB} \quad (39)$$

$$-\overline{V}^2 B_i^{CB}(1 - x_{i,k}^{CB}) \le q_{i,k}^{CB} - B_i^{CB} V_i^{SQ} \le -\underline{V}^2 B_i^{CB}(1 - x_{i,k}^{CB}) \quad (40)$$

$$B_i^{CB}\underline{V}^2 x_{i,k}^{CB} \le q_{i,k}^{CB} \le B_i^{CB}\overline{V}^2 x_{i,k}^{CB} \quad \forall i \in \Omega_N^{CB}, k \in \{1,\cdots,N_i^{CB}\} \quad (41)$$

$$x_{i,k}^{CB} \le x_{i,k-1}^{CB} \qquad \forall i \in \Omega_N^{CB}, k \in \{2,\cdots,N_i^{CB}\} \quad (42)$$

$$\left|\Psi_i^{CB} - \sum_{k=1}^{N_i^{CB}} x_{i,k}^{CB}\right| \le \hat{\delta}_i^{CB} \qquad \forall i \in \Omega_N^{CB} \quad (43)$$

$$x_{i,k}^{CB} \in \{0,1\} \qquad \forall i \in \Omega_N^{CB}, k \in \{1,\cdots,N_i^{CB}\} \quad (44)$$

Constraint (39) provides the total reactive power injection for the CB at node i. The big-M formulation (40) and (41) provides the value of the contribution in the total reactive power injection of each CB module k at node i: if $x_{i,k}^{CB} = 1$, then $q_{i,k}^{CB} = B_i^{CB} V_i^{SQ}$ in (40) and $q_{i,k}^{CB}$ is limited in (41), otherwise, if $x_{i,k}^{CB} = 0$, then $q_{i,k}^{CB} = 0$ in (41) and V_i^{SQ} is limited in (40). Constraint (42) is used to break the symmetry in the model, ensuring that module $k-1$ must be in use to allow the operation of module k. Constraint (43) determines the change in the operation of the CBs, which is penalized in (1). Equation (44) represents the binary nature of $x_{i,k}^{CB}$.

F. Voltage Regulators and On-Load Tap Changers Models

A continuous formulation is used to represent the operation of the VRs and OLTCs. Fig. 1(c) illustrates a branch of the system with a VR. Equation (45) presents the square value of the regulated voltage magnitude at node n as a function of the square value of the voltage magnitude at node i. Equation (46) presents the variable δ_{ij}^{VR}, which represents the difference between the square value of the voltage magnitudes at nodes n and i.

$$V_n^{SQ} = a_{ij}^2 V_i^{SQ} \qquad \forall ij \in \Omega_B^{VR} \quad (45)$$

$$\delta_{ij}^{VR} = V_n^{SQ} - V_i^{SQ} = V_i^{SQ}(a_{ij}^2 - 1) \qquad \forall ij \in \Omega_B^{VR} \quad (46)$$

The tap is $a_{ij} = \Delta_{ij}^{VR} + 1$, in which Δ_{ij}^{VR} is the regulation for the VR of branch ij, therefore, δ_{ij}^{VR} can be defined as shown in (47). Moreover, a_{ij} can be obtained from δ_{ij}^{VR} and V_i^{SQ} as shown in (48).

$$\delta_{ij}^{VR} = \Delta_{ij}^{VR}(\Delta_{ij}^{VR} + 2) V_i^{SQ} \qquad \forall ij \in \Omega_B^{VR} \quad (47)$$

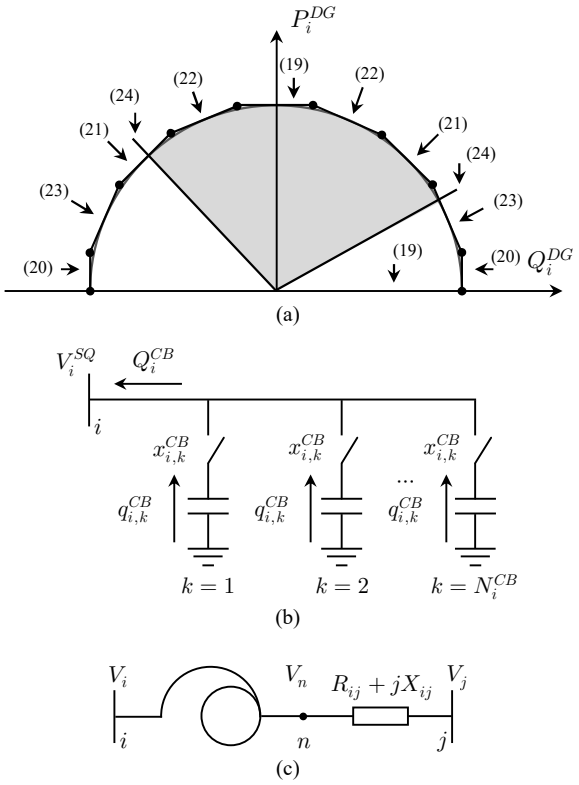

Fig. 1. (a) Linearization of the capacity curve of DGs, (b) illustration of the CBs model, and (c) representation of a branch with a VR.

$$a_{ij} = \frac{\sqrt{V_i^{SQ} + \delta_{ij}^{VR}}}{V_i} \qquad \forall ij \in \Omega_B^{VR} \quad (48)$$

The operation of the VRs is defined by (49) and (50).

$$\left|\delta_{ij}^{VR}\right| \le \overline{\Delta}_{ij}^{VR}\left(2 + \overline{\Delta}_{ij}^{VR}\right) V_i^{SQ} \qquad \forall ij \in \Omega_B^{VR} \quad (49)$$

$$\left|\Psi_{ij}^{VR} V_i^{SQ} - \delta_{ij}^{VR}\vartheta_i^2\right| \le \hat{\delta}_{ij}^{VR} \qquad \forall ij \in \Omega_B^{VR} \quad (50)$$

Constraint (49) presents the limits for δ_{ij}^{VR}, in which $\overline{\Delta}_{ij}^{VR}$ is the value of the maximum regulation for the VR of branch ij, while (50) quantifies the variations of the tap of VRs between the pre-fault and the restored states of the system, in which Ψ_{ij}^{VR} represents the pre-fault value of δ_{ij}^{VR}. Note that, since $\hat{\delta}_{ij}^{VR}$ is minimized in the objective function (1), in (50), the value of $|\Psi_{ij}^{VR} V_i^{SQ} - \delta_{ij}^{VR}\vartheta_i^2|$ will be minimized. The first term of (50) is related to the regulation of the VR before the fault $\Psi_{ij}^{VR} V_i^{SQ} = \Delta_{ij}^{VR}(\Delta_{ij}^{VR}+2)\vartheta_i^2 V_i^{SQ}$, while the second term is calculated by the model for the post-fault operation, $\delta_{ij}^{VR}\vartheta_i^2 = \Delta_{ij}^{VR}(\Delta_{ij}^{VR}+2)V_i^{SQ}\vartheta_i^2$, and since both terms have the common factor $\vartheta_i^2 V_i^{SQ}$, only the difference in the regulation of the VR before and after the fault is accounted for in $\hat{\delta}_{ij}^{VR}$.

Constraints (51) and (52) are used to model the operation of the OLTCs.

$$\left(\left(1 - \overline{\Delta}_i^{OLTC}\right) V^N\right)^2 \le V_i^{SQ} \le \left(\left(1 + \overline{\Delta}_i^{OLTC}\right) V^N\right)^2 \qquad \forall i \in \Omega_N^{SS} \quad (51)$$

$$\left|\Psi_i^{OLTC} - V_i^{SQ}\right| \le \hat{\delta}_i^{OLTC} \qquad \forall i \in \Omega_N^{SS} \quad (52)$$

In (51) and (52), $\overline{\Delta}_{ij}^{OLTC}$ is the maximum regulation of the OLTC at node i and Ψ_i^{OLTC} represents the pre-fault voltage at substation with an OLTC at node i. For a typical VR or OLTC with ±16 positions for the tap and $\overline{\Delta}_{ij}^{VR} = \overline{\Delta}_i^{OLTC} = 0.1$, the maximum error that can be obtained for the voltage regulation is 0.31%; therefore, the formulation presents a good tradeoff between accuracy and complexity.

G. Operational Constraints of Network Assets

The operational constraints of the system are shown in (53)–(61).

$$\underline{V}^2 \le V_i^{SQ} \le \overline{V}^2 \qquad \forall i \in \Omega_N^R \quad (53)$$

$$0 \le I_{ij}^{SQ} \le \overline{I}_{ij}^2 w_{ij}^{SW} \qquad \forall ij \in \Omega_B^R \quad (54)$$

$$\left|P_{ij}\right| \le \overline{VI}_{ij} w_{ij}^{SW} \qquad \forall ij \in \Omega_B^R \quad (55)$$

$$\left|Q_{ij}\right| \le \overline{VI}_{ij} w_{ij}^{SW} \qquad \forall ij \in \Omega_B^R \quad (56)$$

$$0 \le P_i^{SS} \le \overline{S}_i^{SS} \qquad \forall i \in \Omega_N^{SS} \quad (57)$$

$$|Q_i^{SS}| \le \overline{S}_i^{SS} \qquad \forall i \in \Omega_N^{SS} \quad (58)$$

$$|Q_i^{SS}| \le \sqrt{2}\ \overline{S}_i^{SS} - P_i^{SS} \qquad \forall i \in \Omega_N^{SS} \quad (59)$$

$$|Q_i^{SS}| \le \frac{1}{\sin\left(\frac{\pi}{8}\right)} \overline{S}_i^{SS} - \tan\left(\frac{3\pi}{8}\right) P_i^{SS} \qquad \forall i \in \Omega_N^{SS} \quad (60)$$

$$|Q_i^{SS}| \le \frac{1}{\sin\left(\frac{3\pi}{8}\right)} \overline{S}_i^{SS} - \tan\left(\frac{\pi}{8}\right) P_i^{SS} \qquad \forall i \in \Omega_N^{SS} \quad (61)$$

Constraint (53) is the voltage magnitude limit at the nodes, (54)–(56) are the capacities of the branches, and (57)–(61) is the linearization of the capacity of the substations, similar to the linearization presented for the capacity of the DGs.

Constraints (62) and (63) are used to calculate the number of changes in the operational state of the switches.

$$\hat{\delta}_{ij}^{SW} = w_{ij}^{SW} \qquad \forall ij \in \Omega_{SW}^{O} \quad (62)$$

$$\hat{\delta}_{ij}^{SW} = 1 - w_{ij}^{SW} \qquad \forall ij \in \Omega_{SW}^{C} \quad (63)$$

$$w_{ij}^{SW} \in \{0,1\} \qquad \forall ij \in \Omega_{SW}^{R} \quad (64)$$

Constraint (62) is used to identify the switches that are opened, while (63) identify the switches that are closed. Equation (64) indicates the binary nature of w_{ij}^{SW}.

H. Radiality and Microgrid Formation Constraints

The radial topology of the main network and each microgrid is ensured by considering one artificial substation node in the system, which is connected to one node of each section.

Constraint (65) is a necessary condition to impose radiality to the system [2], which is applied to the real and artificial networks together.

$$\sum_{ij \in \Omega_{SW}} w_{ij}^{SW} = |\Omega_{\mathbb{S}}^R| \quad (65)$$

Equation (65) is a sufficient condition if each node is connected to either a real or to the artificial substation. Therefore, by ensuring the existence of a path between each node and a real or the artificial substation, (65) ensures that the main network and each microgrid will present radial topologies.

Constraints (66)–(70) guarantee that, if a section is de-energized, then it must be connected to the artificial substation.

$$\sum_{ji \in \Omega_B} f_{ji}^f - \sum_{ij \in \Omega_B} f_{ij}^f + g_i^f = 1 - y_{\mathbb{S}_i}^{LS} \qquad \forall i \in \Omega_N \quad (66)$$

$$\left|f_{ij}^f\right| \le |\Omega_N| w_{ij}^{SW} \qquad \forall ij \in \Omega_B \quad (67)$$

$$g_i^f = 0 \qquad \forall i \in \Omega_N^R \quad (68)$$

$$0 \le g_i^f \le |\Omega_N| \qquad \forall i \in \Omega_N^F \quad (69)$$

$$\left|y_{\mathbb{S}_i}^{LS} - y_{\mathbb{S}_j}^{LS}\right| \le 1 - w_{ij}^{SW} \qquad \forall ij \in \Omega_{SW}^R \quad (70)$$

Constraint (66) represents an artificial flow balance that ensures that each section of the network is connected to a real or the artificial substation. Constraint (67) is the limit of the artificial flows on branches. Constraint (68) fixes the artificial generation at all the nodes of the system to zero, except at the

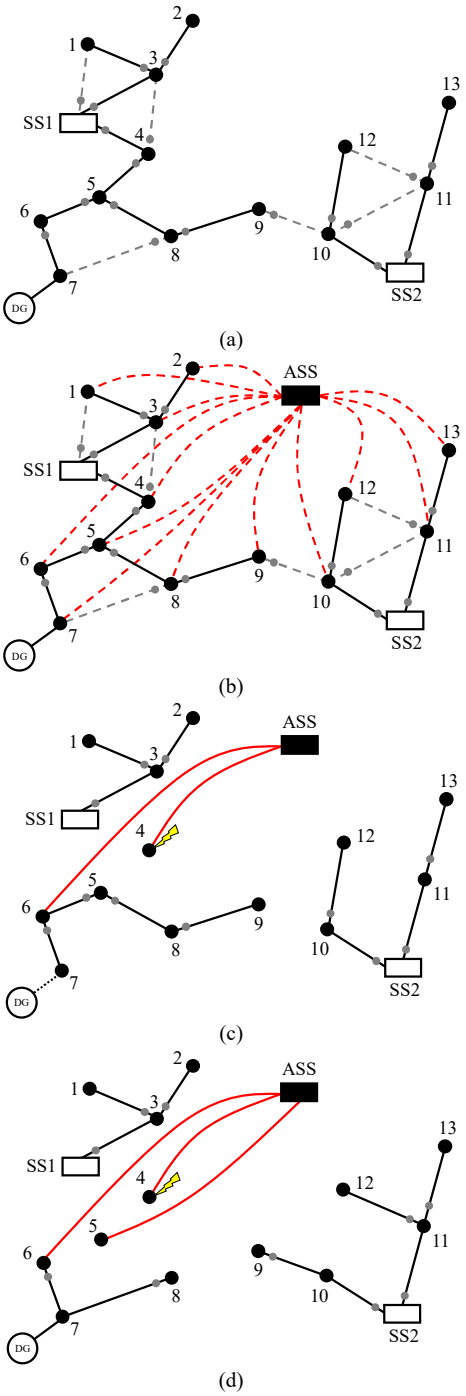

Fig. 2. (a) Illustrative network, (b) illustrative network with the artificial network, (c) faulted system, and (d) resulting restoration scheme with microgrid formation.

artificial substation, while constraint (69) limits the generation at the artificial substation. Constraint (70) guarantees that the statuses of two sections connected by a branch with a switch that is closed are the same.

Constraints (71)–(74) guarantee that if a section is energized, then it must be connected either to a real or the artificial substation. It should be noted that an energized section can only be connected to the artificial substation if its demand is supplied by one or more DGs, operating in microgrid mode.

$$\sum_{ji\in\Omega_B} f^e_{ji} - \sum_{ij\in\Omega_B} f^e_{ij} + g^e_i = y^{LS}_{\mathbb{S}_i} \qquad \forall i \in \Omega_N \qquad (71)$$

$$\left|f^e_{ij}\right| \le |\Omega_N| w^{SW}_{ij} \qquad \forall ij \in \Omega_B \qquad (72)$$

$$g^e_i = 0 \qquad \forall i \in \Omega^D_N \qquad (73)$$

$$0 \le g^e_i \le |\Omega^R_N| \qquad \forall i \in (\Omega^{SS}_N \cup \Omega^F_N) \qquad (74)$$

Constraint (71) represents another artificial flow balance in the system that guarantees that the artificial demands of the energized sections are supplied by the artificial injections from either a real or the artificial substation, defined in (73) and (74). Constraint (72) represents the limits for the flows on the branches.

Fig. 2(a) illustrates a system with thirteen demand nodes, each one representing a section of the system, two substations, SS1 and SS2, and a DG installed at node 7. Fig. 2(b) illustrates the artificial network, which connects each demand node to the artificial substation, ASS. For a fault at the section with node 4, Fig. 2(c) illustrates the resulting configuration after the switches of branches SS1-4, 3-4, and 4-5 are opened to isolate the fault. Nodes 4 and 6 are connected to the artificial substation, and the resulting topology will be radial. As discussed before (see Step 1 of the service restoration procedure in Section II), the DG must be disconnected from the grid, and the power supply is interrupted to sections 5, 6, 7, 8, and 9. Sections 1, 2, 3, 10, 11, 12, and 13, which were not affected by the fault, must remain energized during the service restoration procedure. Fig. 2(d) shows a restoration scheme for the system, considering both reconfiguration and microgrid formation. A microgrid, supplied by the DG at node 7, is formed with nodes 6, 7, and 8, by disconnecting branches 5-6, 5-8, and 8-9, and connecting branch 7-8, while node 9 is connected to SS2 by connecting branch 9-10. Note that, due to operational limits, the part of the system connected to SS2 is reconfigured, so that node 9 is reconnected (branch 10-12 is disconnected and branch 11-12 is connected to the system). This type of operation is not considered in the majority of papers presented in the literature that use mathematical programming formulations to solve the problem, as pointed out in Subsection I-B. Note that the resulting topology, including the artificial network, is radial, and constraints (65)–(74) are satisfied.

Constraints (75)–(82) are used to avoid unnecessary switching operations in the isolated sections.

$$w^{SW}_{ij} \le 1 - z_{ij} \qquad \forall ij \in \Omega^O_{SW} \qquad (75)$$

$$w^{SW}_{ij} \ge z_{ij} \qquad \forall ij \in \Omega^C_{SW} \qquad (76)$$

$$z_{ij} \le 1 - y^{LS}_{\mathbb{S}_i} \qquad \forall ij \in \Omega^R_{SW} \qquad (77)$$

$$z_{ij} \le 1 - y^{LS}_{\mathbb{S}_j} \qquad \forall ij \in \Omega^R_{SW} \qquad (78)$$

$$z_{ij} \ge 1 - y^{LS}_{\mathbb{S}_i} - y^{LS}_{\mathbb{S}_j} \qquad \forall ij \in \Omega^R_{SW} \qquad (79)$$

$$0 \le z_{ij} \le 1 \qquad \forall ij \in \Omega^R_{SW} \qquad (80)$$

$$y^{LS}_{\mathbb{S}_i} = 1 \qquad \forall i \in (\Omega^{SS}_N \cup \Omega^F_N) \qquad (81)$$

$$y^{LS}_{\mathbb{S}_i} = 0 \qquad \forall i \in \Omega^D_N | \mathbb{S}_i \in \Omega^F_{\mathbb{S}} \qquad (82)$$

Constraints (75) and (76) require that the statuses of the switches of the de-energized portions of the network do not change. Constraints (77)–(80) are used to linearize the product $z_{ij} = \left(1 - y^{LS}_{\mathbb{S}_i}\right)\left(1 - y^{LS}_{\mathbb{S}_j}\right)$. Constraint (81) determines the status of $y^{LS}_{\mathbb{S}_i}$ at the substation nodes and constraint (82) requires that the sections under fault must be de-energized.

The MILP model for optimal restoration of distribution systems considering microgrid formation and voltage control devices is composed of (1) subject to (2)–(44) and (49)–(82). Fig. 3 presents the flowchart of the proposed solution approach, which must be implemented on Step 3) of the restoration procedure presented in Section II. Initially, the distribution system data is read. Then, the model (1)–(44) and (49)–(82) is assembled in a mathematical programming language and solved using the branch-and-cut algorithm, available in off-the-shelf optimization solvers for MILP. The solution of the model will present the optimal restoration plan that should be implemented in Step 4) of the restoration procedure.

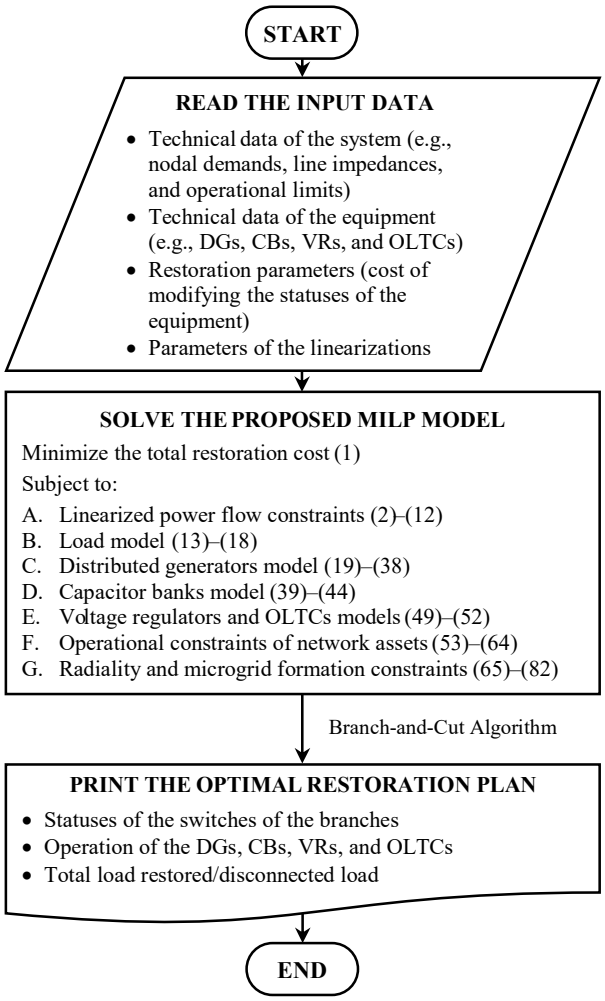

Fig. 3. Flowchart of the proposed solution approach.

IV. Tests and Results

A 53-node system adapted from [3] and shown in Fig. 4 is used to test the proposed model. The system has three substations and 50 load nodes, each one representing a section. It is considered that each branch is equipped with a switch. Six DGs with capacities of 3,000 kVA, 6,500 kVA, 8,000 kVA, 4,000 kVA, 8,000 kVA, and 5,000 kVA are installed at nodes 2, 16, 20, 36, 43, and 49, respectively. All the DGs, except the ones at nodes 16 and 36, have black-start capacity. For all the DGs, it is assumed that $\bar{\tau}_i^{cap} = \bar{\tau}_i^{ind} = 0.85$. Three CBs, with four modules of 300 kVAr (at nominal voltage) each, are installed at nodes 26, 29, and 32. All the substations are equipped with OLTCs with a total regulation of 10% and ±16 tap positions. Four VRs, with regulation of 10% and ±16 tap positions, are installed at branches 4-5, 22-23, 38-39, and 42-47. The nominal voltage at the substations is 13.8 kV, while the minimum and maximum voltage magnitude limits are 0.95 p.u. and 1.05 p.u., respectively. Complete data for this system is available in [33]. The values adopted for the parameters of the objective function are $\kappa_i^{LS} = 100$ US$/kW, $\kappa_{ij}^{SW} = 10$ US$, $\kappa_i^{DGp} = 0.01$ US$/kW, $\kappa_i^{DGq} = 0.01$ US$/kVAr, $\kappa_i^{CB} = 1$ US$, $\kappa_i^{OLTC} = 1$ US$, and $\kappa_{ij}^{VR} = 1$ US$, and $\kappa^{MG} = 100$ US$. These costs are selected so that the load not supplied becomes the term with the highest priority. The number of blocks used in the piecewise linearization is $\Lambda = 15$.

Three fault cases are considered. In Case A, faults at sections {1, 3, 11, 14} are considered, which isolate substations 101 and 102. The restorable load, in this case, is 52,740.07 kW. In Case B, faults at sections {1, 3, 21, 22, 30} are considered, which isolate substations 101 and 103. The restorable load, in this case, is 34,228.66 kW. In Case C, faults at sections {1, 3, 11, 14, 21, 22, 30} are considered, which isolate all substations. The restorable load, in this case, is 63,101.81 kW. In order to analyze the impact of microgrid formation and voltage control on the restoration problem, three different approaches are applied to each case: 1) considering network reconfiguration, microgrid formation, and voltage control; 2) considering network reconfiguration and microgrid formation, while disregarding voltage control, i.e., the tap positions of the OLTCs and VRs, and the number of CBs modules connected at each node remain the same as the values of the

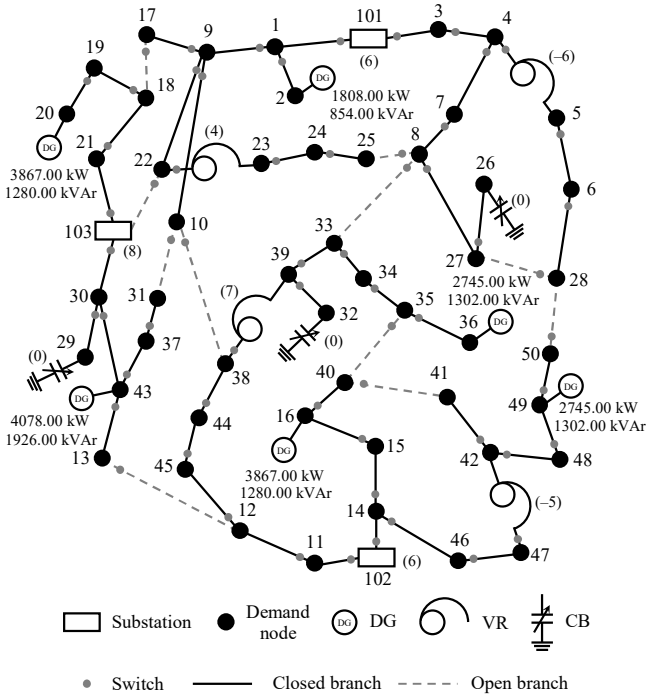

Fig. 4. Pre-fault configuration of the 53-node system.

TABLE II
Summary of the Solutions

Case	Switches opened	Switches closed	Active load restored (%)
A1	1-9, 1-101, 3-4, 3-101, 6-28, 9-10, 9-17, 11-12, 11-102, 14-15, 14-46, 14-102, 34-35, 44-45, 46-47	12-13, 17-18, 22-103, 28-50, 35-40, 40-41	47.02
A2	1-2, 1-9, 1-101, 3-4, 3-101, 5-6, 9-10, 9-17, 11-12, 11-102, 14-15, 14-46, 14-102, 22-23, 30-43, 34-35, 42-47	17-18, 22-103, 28-50, 35-40, 40-41	35.32
A3	1-2, 1-9, 1-101, 3-4, 3-101, 11-12, 11-102, 14-15, 14-46, 14-102	–	0.00
B1	1-2, 1-9, 1-101, 3-4, 3-101, 6-28, 7-8, 9-22, 15-16, 18-21, 21-103, 22-23, 29-30, 30-43, 30-103, 42-48	8-33, 12-13, 27-28, 28-50, 35-40	52.38
B2	1-2, 1-9, 1-101, 3-4, 3-101, 5-6, 9-22, 15-16, 18-21, 21-103, 22-23, 29-30, 30-43, 30-103, 37-43, 42-47	12-13, 28-50, 35-40, 40-41	29.59
B3	1-2, 1-9, 1-101, 3-4, 3-101, 5-6, 9-22, 15-16, 18-21, 21-103, 22-23, 29-30, 30-43, 30-103, 37-43, 42-47	12-13, 28-50, 35-40, 40-41	12.93
C1	1-2, 1-9, 1-101, 3-4, 3-101, 6-28, 9-22, 11-12, 11-102, 14-15, 14-46, 14-102, 18-21, 21-103, 22-23, 29-30, 30-43, 30-103, 34-35, 46-47	28-50, 35-40, 40-41	40.41
C2	1-2, 1-9, 1-101, 3-4, 3-101, 5-6, 9-22, 11-12, 11-102, 14-15, 14-46, 14-102, 18-21, 21-103, 22-23, 29-30, 30-43, 30-103, 34-35, 42-47	28-50, 35-40, 40-41	39.85
C3	1-2, 1-9, 1-101, 3-4, 3-101, 9-22, 11-12, 11-102, 14-15, 14-46, 14-102, 18-21, 21-103, 22-23, 29-30, 30-43, 30-103	–	0.00

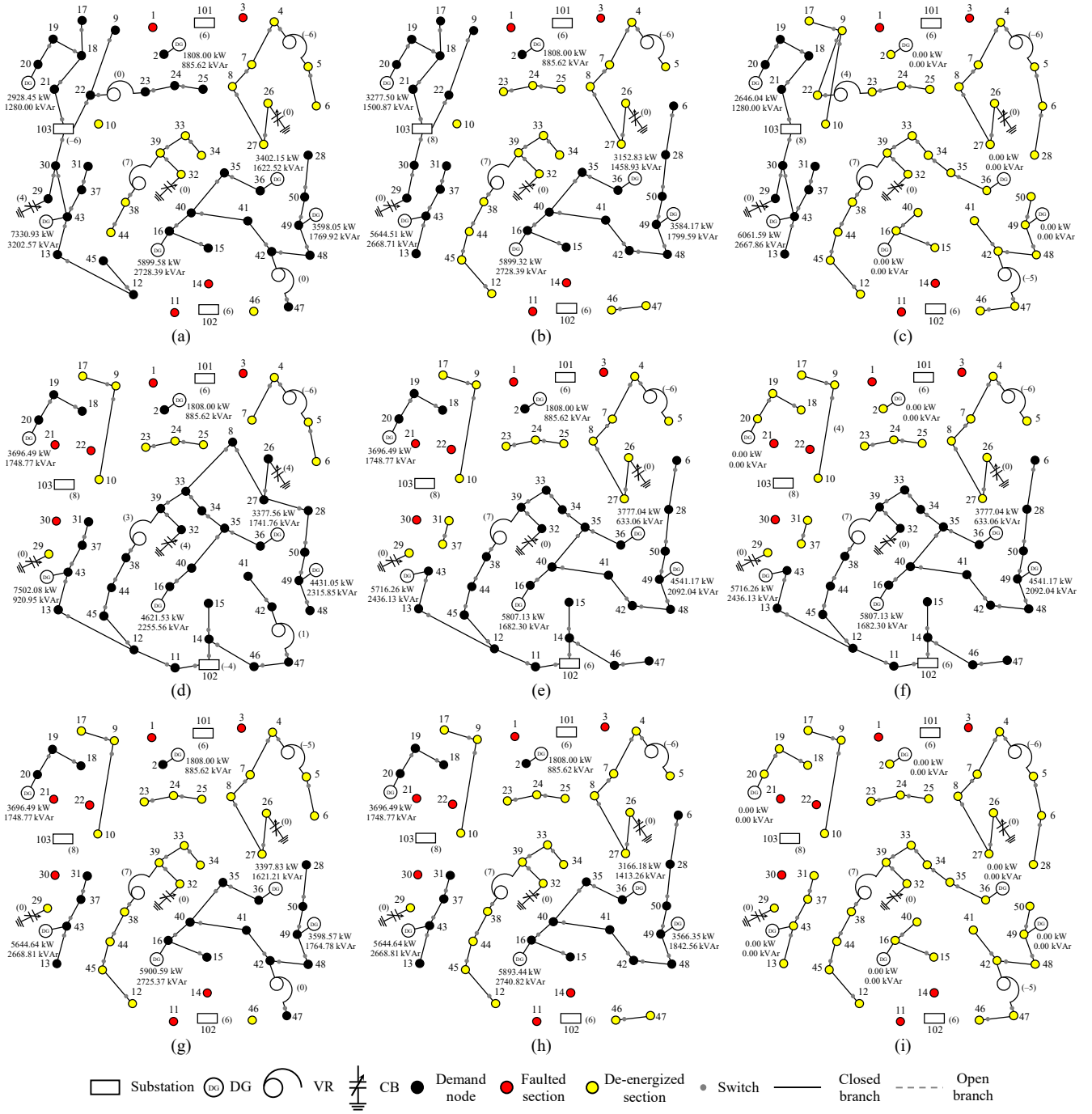

Fig. 5. Operation of the system for Case (a) A1, (b) A2, (c) A3, (d) B1, (e) B2, (f) B3, (g) C1, (h) C2, and (i) C3.

pre-fault configuration; and 3) considering only network reconfiguration, thereby disregarding microgrid formation, which requires the connected operation of the DGs, and voltage control.

The main results for each case are summarized in Table II, which shows the switching operations and the percentage of active load restored in terms of the restorable load affected by the faults (without considering the load at the faulted sections), while Fig. 5(a)–(i) shows the details of the operation of the system for each case. In Fig. 5, the red nodes (sections) are the faulted sections, the yellow nodes are the de-energized sections, and the black nodes are the energized sections. Moreover, the numbers in brackets refer to the tap positions of VRs and substations' OLTCs, and the number of CB modules in operation. The active and reactive power generations of the DGs are shown for each DG.

The optimization model was implemented in AMPL [34] and solved with the commercial solver CPLEX v20.1.0 [35], with default settings, on a computer with a 2.80 GHz Intel® Core™ i7–7700HQ processor and 16 GB of RAM.

By analyzing the results presented in Table II and Fig. 5, it is possible to verify that, in Case A1, nine switching operations are performed to isolate the faulted sections and twelve operations are performed to restore the service to the affected nodes, by reconfiguring the system and forming the microgrids. As it can be observed in Fig. 5(a), two microgrids are formed in the system. One microgrid is formed with the DGs of nodes 16 and 36, which do not have the black-start capacity, connected to the DG of node 49, with black-start capacity. Microgrids with these three DGs interconnected are also verified in Cases A2 (Fig. 5(b)), C1 (Fig. 5(g)), and C2 (Fig. 5(h)). The other microgrid is formed with only the DG

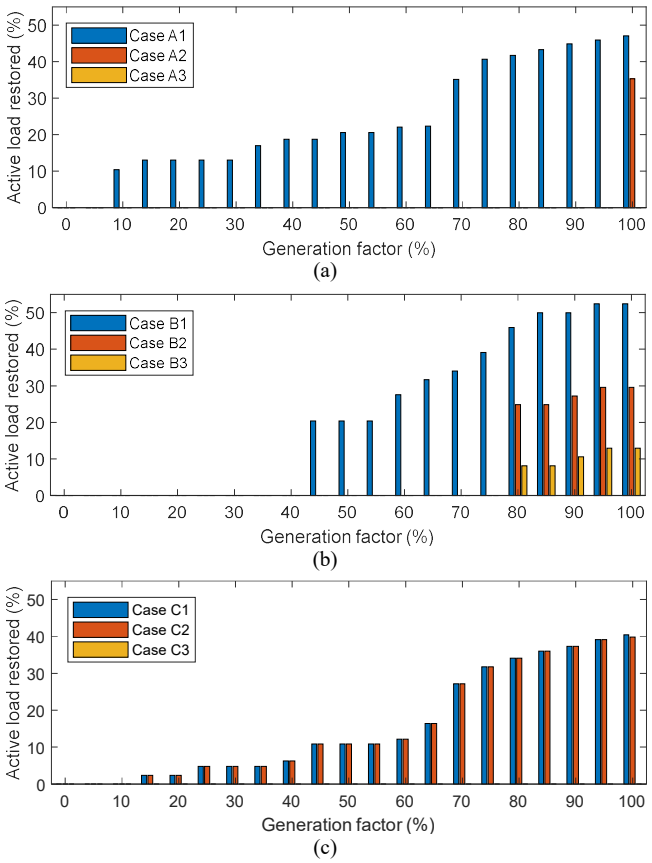

Fig. 6. Sensitivity analysis of the generation capacities for (a) Case A, (b) Case B, and (c) Case C.

at node 2, which can also be verified in Cases A2, B1, B2, C1, and C2. The active load restored in Case A1 is 47.02%, which is reduced to 35.32% in Case A2 by not considering voltage control. In Case A2 the system operates with three microgrids (see Fig. 5(b)). In Case A3, microgrid formation is not allowed, no load affected by the fault can be restored, and all sections that were de-energized due to the faults must remain isolated until the faults have been cleared, as shown in Fig. 5(c).

In Case B1, nine switching operations are performed to restore the service, in addition to the thirteen operations to isolate the faulted sections. As shown in Fig. 5(d), the system operates with two microgrids, and 52.38% of the affected load is restored. Also, note that in this case, as in Case B2 (see Fig. 5(e)), the DGs at nodes 16, 36, 43, and 49 operate connected to the portion of the network supplied by substation 102. In Case B2, two microgrids are formed in the network with eight switching operations, besides the thirteen operations to isolate the faulted sections, and 22.79% less load affected by the faults is restored in comparison to Case B1. In Case B3 (Fig. 5(f)), eight switching operations are performed (besides the ones to isolate the fault) and the active load restored is reduced to 12.93%. The results of Cases A1–A3 and B1–B3 make clear the advantages of considering voltage control and microgrid formation in the service restoration problem since more load can be restored when all these actions, together with network reconfiguration, are allowed in the problem.

In Case C1 (see Fig. 5(g)), six switching operations are performed, besides the seventeen operations performed to isolate the faulted sections. Four microgrids are formed in the network, and 40.41% of the active load is restored. By not considering voltage control in the problem, Case C2 (Fig. 5(h)) shows that 0.56% less load affected by the faults is restored in comparison to the solution of Case C1, while the same number of switching operations of Case C1 is performed, and four microgrids are formed in the system. In Case C3, as in Case A3, no load can be restored, indicating again the importance of considering microgrid formation in the service restoration problem.

The results, therefore, demonstrate the importance of considering the optimization of voltage control devices in the service restoration problem together with reconfiguration and microgrid formation strategies, in order to attain high-quality restoration schemes. In all three cases, it can be verified a tendency of the OLTCs and VRs to reduce the voltage in the system, thereby reducing the voltage-dependent load.

The computational times to solve Cases A1–C3 are, respectively, 22.47 s, 30.08 s, 2.45 s, 1.73 s, 0.91 s, 0.66 s, 0.98 s, 0.91 s, and 0.13 s, which are adequate to the time frame of the service restoration problem.

A sensitivity analysis was carried out to analyze the influence of the total DG capacity on the active load restored. Fig. 6 shows how the active load restored varies as a function of the DG capacity of the system, when their values are simultaneously increased from zero (generation factor of 0%) until $\overline{S}_i^{DG}$ (generation factor of 100%) in each case considered before. The values of Ψ_i^{DGp} and Ψ_i^{DGp} are also multiplied by the same generation factor in each case.

Fig. 6(a) again shows the importance of considering voltage control in the restoration problem. For Case A1, the total load restored increases from 10.38% when all DGs' capacities are reduced to 10% of their values up to 47.02% when their full capacities are considered. In Case A2, it is only possible to restore the service to part of the de-energized load when the full capacities of the DGs are considered. It should be mentioned that, in this case, with the reduced capacities of the DGs and without the possibility of voltage control, even the operation of the sections that were not affected by the faults, and must remain energized, become infeasible. In Case A3, it is not possible to restore the service to any load for any generation factor. Fig. 6(b) also shows that by considering voltage control simultaneously with microgrid formation, more load can be restored when the capacities of the DGs are reduced. In Fig. 6(c) it can be verified that the results for Case C2 present almost the same values of total load restored as Case C1. This can be explained by the fact that almost all voltage control devices are installed in the sections that remain de-energized in the solution of the problem, as can be verified in Fig. 5(g) and (h).

Finally, it should be highlighted that all the solutions obtained in this work were evaluated using an exact power flow algorithm, which demonstrated their feasibility, indicating the precision of the model.

V. Conclusion

This paper presented a new mixed-integer linear programming model for the problem of optimal restoration of active distribution systems considering network reconfiguration, microgrid formation, and voltage control devices. The proposed approach accounted for both the black-start capacity of generators and the connection of multiple generators to the same microgrid. The objective was to analyze the impact of voltage control and microgrid formation on the restoration problem.

A 53-node system with three substations was used to test the model. Three severe fault cases were considered, disconnecting two substations from the system in the first two cases

and all three substations in the last case. For each case, three approaches were evaluated for the restoration problem, in which the first one considered microgrid formation and voltage control, the second one did not consider voltage control, and the last one did not consider both microgrid formation and voltage control. The results indicated that by considering voltage control in the problem together with microgrid formation, more load could be restored in all the cases tested.

A sensitivity analysis was carried out to analyze the impact of the distributed generators' capacities in the restoration problem. The obtained results again showed the importance of considering voltage control in the service restoration problem together with microgrid formation, since more load can be restored when the capacities of the distributed generators are reduced.

The proposed model was effective to solve the problem, presenting a good tradeoff between precision and computational times. Note that a power flow analysis indicated that all the results were feasible whereas the computational times to solve the problem were very low.

Future work will analyze the impact on the system's reliability of different restoration strategies, including the ones presented in this paper and others, such as demand-side management and meshed operation of the network. Further research will also address the consideration of renewable energy resources with uncertain outputs.

References

[1] L. H. Macedo, G. Muñoz-Delgado, J. Contreras, and R. Romero, "Optimal service restoration in active distribution networks considering microgrid formation and voltage control devices," in *2020 International Conference on Smart Energy Systems and Technologies (SEST)*, 2020, pp. 1–6.

[2] A. Zidan *et al.*, "Fault detection, isolation, and service restoration in distribution systems: state-of-the-art and future trends," *IEEE Trans. Smart Grid*, vol. 8, no. 5, pp. 2170–2185, Sep. 2017.

[3] R. Romero, J. F. Franco, F. B. Leão, M. J. Rider, and E. S. de Souza, "A new mathematical model for the restoration problem in balanced radial distribution systems," *IEEE Trans. Power Syst.*, vol. 31, no. 2, pp. 1259–1268, Mar. 2016.

[4] Y. Li, J. Xiao, C. Chen, Y. Tan, and Y. Cao, "Service restoration model with mixed-integer second-order cone programming for distribution network with distributed generations," *IEEE Trans. Smart Grid*, vol. 10, no. 4, pp. 4138–4150, Jul. 2019.

[5] Y. Wang, C. Chen, J. Wang, and R. Baldick, "Research on resilience of power systems under natural disasters—a review," *IEEE Trans. Power Syst.*, vol. 31, no. 2, pp. 1604–1613, Mar. 2016.

[6] L. Jikeng *et al.*, "Two-stage method for optimal island partition of distribution system with distributed generations," *IET Gener. Transm. Distrib.*, vol. 6, no. 3, pp. 218–225, Mar. 2012.

[7] C. Chen, J. Wang, F. Qiu, and D. Zhao, "Resilient distribution system by microgrids formation after natural disasters," *IEEE Trans. Smart Grid*, vol. 7, no. 2, pp. 958–966, Mar. 2016.

[8] V. Hosseinnezhad, M. Rafiee, M. Ahmadian, and P. Siano, "Optimal island partitioning of smart distribution systems to improve system restoration under emergency conditions," *Int. J. Electr. Power Energy Syst.*, vol. 97, pp. 155–164, Apr. 2018.

[9] T. Khalili, M. T. Hagh, S. G. Zadeh, and S. Maleki, "Optimal reliable and resilient construction of dynamic self-adequate multi-microgrids under large-scale events," *IET Renew. Power Gener.*, vol. 13, no. 10, pp. 1750–1760, Jul. 2019.

[10] S. Ghasemi, A. Khodabakhshian, and R.-A. Hooshmand, "Decision-making method for critical load restoration by using MGs," *IET Gener. Transm. Distrib.*, vol. 13, no. 20, pp. 4630–4641, Oct. 2019.

[11] T. Khalili, A. Bidram, and M. J. Reno, "Impact study of demand response program on the resilience of dynamic clustered distribution systems," *IET Gener. Transm. Distrib.*, vol. 14, no. 22, pp. 5230–5238, Nov. 2020.

[12] L. Fu, B. Liu, K. Meng, and Z. Y. Dong, "Optimal restoration of an unbalanced distribution system into multiple microgrids considering three-phase demand-side management," *IEEE Trans. Power Syst.*, vol. 36, no. 2, pp. 1350–1361, Mar. 2021.

[13] S. Cai, Y. Xie, Q. Wu, M. Zhang, X. Jin, and Z. Xiang, "Distributionally robust microgrid formation approach for service restoration under random contingency," *IEEE Trans. Smart Grid*, pp. 1–11, 2021.

[14] J. Li, X.-Y. Ma, C.-C. Liu, and K. P. Schneider, "Distribution system restoration with microgrids using spanning tree search," *IEEE Trans. Power Syst.*, vol. 29, no. 6, pp. 3021–3029, Nov. 2014.

[15] Y. Xu, C.-C. Liu, K. P. Schneider, F. K. Tuffner, and D. T. Ton, "Microgrids for service restoration to critical load in a resilient distribution system," *IEEE Trans. Smart Grid*, vol. 9, no. 1, pp. 426–437, Jan. 2018.

[16] K. S. A. Sedzro, A. J. Lamadrid, and L. F. Zuluaga, "Allocation of resources using a microgrid formation approach for resilient electric grids," *IEEE Trans. Power Syst.*, vol. 33, no. 3, pp. 2633–2643, May 2018.

[17] F. Wang *et al.*, "Service restoration for distribution network with DGs based on stochastic response surface method," *Int. J. Electr. Power Energy Syst.*, vol. 107, pp. 557–568, May 2019.

[18] S. H. Alemohammad, E. Mashhour, and H. Farzin, "Two-stage market-based service restoration method in multi-MGs distribution networks," *IET Gener. Transm. Distrib.*, vol. 13, no. 23, pp. 5375–5386, Dec. 2019.

[19] Y. Wang *et al.*, "Coordinating multiple sources for service restoration to enhance resilience of distribution systems," *IEEE Trans. Smart Grid*, vol. 10, no. 5, pp. 5781–5793, Sep. 2019.

[20] S. Lei, C. Chen, Y. Song, and Y. Hou, "Radiality constraints for resilient reconfiguration of distribution systems: formulation and application to microgrid formation," *IEEE Trans. Smart Grid*, vol. 11, no. 5, pp. 3944–3956, Sep. 2020.

[21] F. W. Glover and G. A. Kochenberger, *Handbook of Metaheuristics*. Boston, MA, USA: Kluwer Academic Publishers, 2003.

[22] T. Gönen, *Electric power distribution engineering*, 3rd ed. Boca Raton: CRC Press, 2014.

[23] A. Majumdar, Y. P. Agalgaonkar, B. C. Pal, and R. Gottschalg, "Centralized volt–var optimization strategy considering malicious attack on distributed energy resources control," *IEEE Trans. Sustain. Energy*, vol. 9, no. 1, pp. 148–156, Jan. 2018.

[24] R. W. Uluski, "VVC in the smart grid era," in *IEEE PES General Meeting*, 2010, pp. 1–7.

[25] R. A. V. Peralta, J. B. Leite, and J. R. S. Mantovani, "Automatic restoration of large-scale distribution networks with distributed generators, voltage control devices and heating loads," *Electr. Power Syst. Res.*, vol. 176, pp. 1–11, Nov. 2019.

[26] H. Sekhavatmanesh and R. Cherkaoui, "Analytical approach for active distribution network restoration including optimal voltage regulation," *IEEE Trans. Power Syst.*, vol. 34, no. 3, pp. 1716–1728, May 2019.

[27] D. Fan, Y. Ren, Q. Feng, Y. Liu, Z. Wang, and J. Lin, "Restoration of smart grids: Current status, challenges, and opportunities," *Renew. Sustain. Energy Rev.*, vol. 143, no. January, p. 110909, Jun. 2021.

[28] B. Chen, J. Wang, X. Lu, C. Chen, and S. Zhao, "Networked microgrids for grid resilience, robustness, and efficiency: A review," *IEEE Trans. Smart Grid*, vol. 12, no. 1, pp. 18–32, Jan. 2021.

[29] Z. Shuai *et al.*, "Microgrid stability: classification and a review," *Renew. Sustain. Energy Rev.*, vol. 58, pp. 167–179, May 2016.

[30] F. Goulart, A. L. Maravilha, E. G. Carrano, and F. Campelo, "Permutation-based optimization for the load restoration problem with improved time estimation of maneuvers," *Int. J. Electr. Power Energy Syst.*, vol. 101, pp. 339–355, Oct. 2018.

[31] R. R. Gonçalves, R. P. Alves, J. F. Franco, and M. J. Rider, "Operation planning of electrical distribution systems using a mixed integer linear model," *J. Control. Autom. Electr. Syst.*, vol. 24, no. 5, pp. 668–679, Oct. 2013.

[32] L. M. Hajagos and B. Danai, "Laboratory measurements and models of modern loads and their effect on voltage stability studies," *IEEE Trans. Power Syst.*, vol. 13, no. 2, pp. 584–592, May 1998.

[33] L. H. Macedo, G. Muñoz-Delgado, J. Contreras, and R. Romero, "Optimal service restoration in active distribution networks considering microgrid formation and voltage control devices: test data," 2021. [Online]. Available: http://ieee-dataport.org/4204. [Accessed: 07-May-2021].

[34] R. Fourer, D. M. Gay, and B. W. Kernighan, *AMPL: A modeling language for mathematical programming*, 2nd ed. Duxbury, MA, USA: Thomson, 2003.

[35] IBM, "IBM ILOG CPLEX Optimization Studio 20.1.0 documentation," *2021*. [Online]. Available: https://www.ibm.com/support/knowledgecenter/SSSA5P_20.1.0/COS_KC_home.html. [Accessed: 01-Feb-2021].

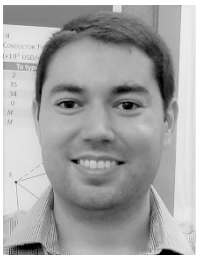

Leonardo H. Macedo (S'14–M'18) (S'14–M'18) received the B.S., M.S., and Ph.D. degrees, all in Electrical Engineering, from the São Paulo State University, São Paulo, Brazil, in 2012, 2015, and 2019, respectively, where he is currently a postdoctoral researcher. During 2016–2017, he was a visiting student at the University of Washington, Seattle, USA, and from 2019–2020 he was a post-doctoral researcher at the Universidad de Castilla-La Mancha, Ciudad Real, Spain.

His current research interests include the development of methods for the optimization, planning, and control of electrical power systems.

Gregorio Muñoz-Delgado (S'14–M'18) received the Ingeniero Industrial degree, the M.Sc. degree, and the Ph.D. degree from the Universidad de Castilla-La Mancha, Ciudad Real, Spain, in 2012, 2013, and 2017, respectively.

He is currently an Associate Professor with the Universidad de Castilla-La Mancha, Ciudad Real, Spain. His research interests are in the fields of power systems planning, operation, and economics.

Javier Contreras (SM'05–F'15) received the B.S. degree in electrical engineering from the University of Zaragoza, Zaragoza, Spain, in 1989, the M.Sc. degree from the University of Southern California, Los Angeles, CA, USA, in 1992, and the Ph.D. degree from the University of California, Berkeley, CA, USA, in 1997.

He is a Professor with the Universidad de Castilla-La Mancha, Ciudad Real, Spain. His research interests include power systems planning, operation, and economics, as well as electricity markets.

Rubén Romero (M'93–SM'08) received the B.Sc. in Electrical Engineering and P.E. degrees from the National University of Engineering, Lima, Peru, in 1978 and 1984, respectively. He received the M.Sc. and Ph.D. degrees from the University of Campinas, Campinas, Brazil, in 1990 and 1993, respectively. He is currently a professor of electrical engineering at the São Paulo State University, Ilha Solteira, Brazil.

His research interests include methods for the optimization, planning, and control of electrical power systems, applications of artificial intelligence in power systems, and operations research.